ANALYSIS OF THE NONLINEAR PARAMETER IN INVERSE PROBLEMS OF ELASTICITY

A Thesis

by

SHANKAR LALITHA SRIDHAR

Submitted to the Office of Graduate and Professional Studies of
Texas A&M University
in partial fulfillment of the requirements for the degree of

MASTER OF SCIENCE

Chair of Committee,	Sevan Goenezen
Committee Members,	Raffaella Righetti
	Alan Freed
Head of Department,	Andreas A. Polycarpou

December 2016

Major Subject: Mechanical Engineering

ABSTRACT

The mechanical properties of tissues are important indicators of tissue "health". It has been recorded and acknowledged that diseased tissues due to cancer or other conditions tend to stiffen with increase in strain, exhibiting a nonlinear stress-strain behavior. In literature, hyperelastic models, such as Veronda-Westmann and Blatz, have been widely used to model soft tissues. These models are characterized by an exponential function and two material parameters, namely the shear modulus μ and a nonlinearity parameter γ. A variety of methods and techniques have been developed to solve inverse problems in elasticity to determine these properties given the mechanical response of the tissues. Reconstruction of the nonlinear parameter using noisy measured displacement data is a difficult problem, and obtaining a well-posed solution is a challenge. This thesis is directed towards the improvement in the reconstruction of the nonlinear parameter, γ, by introducing a new parameter, which is a combination of γ and the first invariant of the Green deformation tensor. Comparative study is carried out between reconstructions of γ directly from previously existing formulations and the reconstruction of γ from the new parameter, for 2D problems. Numerical experiments are conducted and the performance is tested and compared based on different criteria like shape of the stiff regions (representing the diseased tissue), the contrast in γ and robustness for different loading conditions. Different arrangements and sizes of stiff inclusions are tested and critically analyzed. It is found that obtaining the distribution of γ from the new parameter results in a much better reconstruction than by directly optimizing for γ.

DEDICATION

To my parents

ACKNOWLEDGEMENTS

I would like to thank my committee chair and my advisor, Dr. Goenezen for his guidance and support throughout the course of this research.

I am grateful to the friends I made who made my stay at College Station enjoyable even though I was far away from home. I am thankful to Yue Mei, my lab mate, for helping me with a smooth transition into this research field which was new to me. I would also like to thank the Department of Mechanical Engineering and Texas A&M for the financial support during the course of my study here.

Finally, thanks to my family for their unwavering support and guidance during my stay here.

TABLE OF CONTENTS

Page

LIST OF FIGURES

Page

CHAPTER I

INTRODUCTION

Mechanical behavior of soft tissues has been studied in detail to provide better understanding on identification of abnormalities. The most commonly used method of detection presently is strain imaging. However, detecting abnormalities due to lesions and tumors based on the actual material properties would characterize the disease more accurately than just based on strain variations. Elasticity imaging or elastography introduced first by Ophir et al [1] is a medical imaging technique to approximate the elastic stiffness distribution of the tissue based on tissue motion, to help identify diseased regions. Tissue motion i.e. displacement data and strains can be obtained using different imaging modalities like ultrasound imaging, Magnetic Resonance Imaging (MRI) or Computed Tomography (CT), out of which ultrasound imaging has been most widely studied (see [2] - [7]).

1.1 Linear Elasticity Imaging

Broadly speaking the elastic properties of tissues are obtained using data from the deformation of tissues by two methods. One is the direct method where the elastic modulus is solved directly from the equations of equilibrium assuming a linear elastic solid (see [6], [8] - [11]). The other is the iterative method where a least squares formulation is used to minimize the error in measured and computed displacement fields. Unlike the direct method, the iterative method can be used in the case of a linear elastic solid as well as nonlinear hyperelastic solids.

While the direct method might be an efficient solution to the inverse problem it has serious drawbacks. This approach requires taking derivatives of noisy displacement data, which significantly amplifies noise and compromises the accuracy of the solution. Additionally, in these methods it is assumed that the material is linear elastic and the strains are small which is rarely true with most cases in reality. Moreover, some direct methods obtain the "elasticity" image by just inverting the strain image obtained from ultrasound data (see [1] - [2], [4]). With these methods there are possibilities of undesired artifacts because of the non-homogeneity of the tissues, as a result of the assumption that the stress is constant in the problem domain which, strictly speaking, is not valid.

A minimization algorithm is used in iterative methods, where the difference in the measured and computed displacement fields in the L-2 norm is minimized subjected to the constraint that the computed displacement field satisfies the forward problem for a given distribution of material properties. The algorithm is used to obtain the right distribution of material properties that minimizes the error in the displacement fields. However, in iterative methods, the calculation of a Jacobian to compute gradients as part of the algorithm renders the method computationally expensive (see [12] - [15]). Oberai et al introduced adjoint based elasticity equations to calculate the gradients required for a quasi-Newton optimization scheme ([16], [17], [40]). The adjoint equations have been shown to save a lot of computational effort (see references for more details).

Noise in the displacement data is handled by introducing a regularization term in the objective function that serves to reduce fluctuations in the material distribution arising as a result of measurement noise. Though the iterative methods can handle noise better,

the level of noise in the lateral displacements obtained from imaging devices can be so high that it is usual practice to omit them in the inverse problem formulation. However, this reduces the information used in the problem and can affect the uniqueness of the solution.

To overcome the problem of higher noise level in the lateral displacements than axial displacements, Babaniyi et al developed a sparse relaxation method where the momentum equation is relaxed and the lateral displacement and strains are reconstructed for a linear elastic material without using any knowledge of the material stiffness [18]. The lateral displacement data together with the measured axial displacement data is then used for reconstructing the material stiffness.

1.2 Elasticity Parameter Estimation by Error in Constitutive Equation

Iterative methods with alternate minimization functions such as the error in the constitutive equation have been proposed in recent works. The constitutive equation gap method initially proposed by Geymonat [19] was used by Florentin [20] to reconstruct a heterogeneous distribution of elastic properties using a linear elastic model based on full field measurements. This method uses a minimization scheme with a two-step process that minimizes an error functional interpreted as an error in constitutive relation. It is defined as the difference between an admissible stress field and stress calculated from an admissible displacement field. This formulation of minimizing the error in the constitutive equation has also been extended to involve dynamic data induced by mechanical vibrations [21, 22] and to obtain the viscoelastic properties of tissues [23]. Guchhait et al

[24] extended the inversion method to the nonlinear regime for different hyperelastic materials with quasi-static loading.

1.3 Elasticity Imaging for Nonlinear Model Behavior

Studies have shown that tissues exhibit nonlinear behavior to mechanical stimuli at finite strains. The nonlinear behavior is important to identify and differentiate healthy tissues and diseased tissues like cancerous lesions [25,26]. The physiological functioning of several tissues like arterial walls, cartilage etc. have been found to exhibit nonlinear behavior [27]. The underlying pathology of ex vivo breast tissues has been shown to depend on the degree of nonlinearity of the stress-strain relationship for the material [28, 29].

Breast tissues with malignant tumors are found to be much stiffer than a healthy tissue, at large strains. Therefore, determining the material parameters which govern the nonlinearity of the tissue is crucial in identifying cancerous lesions. Driven by the above finding of the importance of capturing the nonlinear behavior of tissues, there have been studies by several groups on *in vivo* tissues taking into account the heterogeneity induced by tumors. Nitta and Shiina proposed to quantify the nonlinear response of *in vivo* tissues by means of images which depict the slope of the strain contrast in the domain with the applied strain [30]. However, the model treats the tissue response as uniaxial and does not consider geometric nonlinearity. The study of geometric nonlinearity with a linear elastic material law (Hooke's law) in tissues was undertaken by Skovoroda and Erkamp ([31] - [34]). Skovoroda et al [32] obtained an estimate of the nonlinearity of tissues by introducing a strain hardening parameter which is some kind of a "strain-slope" image

similar to Nitta and Shiina [30]. The geometric nonlinearity at large deformations is taken into account by Skovoroda et al [34], where the mechanical equilibrium is formulated as a PDE in the shear modulus μ with strains calculated from the measured displacement fields. The issue of noisy displacements, that creates a difficult problem to solve, is handled by performing an incompressibility processing (see [35]) to obtain a reasonably smooth lateral displacement as opposed to an extremely noisy and inaccurate measured displacement field in the lateral direction. This is done assuming availability of axial displacement data with a small noise level and an extremely noisy lateral displacement field.

Hagan and Samani modeled the breast tissue based on different hyperelastic models, in particular Yeoh, polynomial, Ogden, Arruda-Boyce, and Veronda-Westmann and solved for the parameters of the models by matching an experimental force and a simulated force ([36] and [37]). The tissue surrounding the tumor was assumed to be known and the properties of the tumor was determined to capture the nonlinear biomechanical behavior of various types of benign and malignant tumors. It assumes the location of tumors to be known and their elastic properties to be constant throughout the tumor. However, it provides insight into the nonlinear mechanical behavior of different tumor types.

The heterogeneous material properties based on hyperelastic models such as the modified Veronda Westmann model and the modified Blatz models were recovered for incompressible soft tissues under assumptions of plane stress and plane strain [38] - [39]. These papers also provide an estimate of how large the strain should be, at a given noise

level, for the nonlinear signal to be prominent enough to enable good reconstruction of the nonlinear parameter. The technique was applied to breast patient data at large deformations to identify tumors in breast tissues based on the values of the nonlinear parameter (see [40]).

In all these studies the reconstruction of the nonlinear parameter is found to be more sensitive to noise than the shear modulus. Solving the inverse problem for the nonlinear parameter, especially at medium strains when the nonlinear signal is not that pronounced, requires a better method.

1.4 Organization of Thesis

In this thesis, a new parameter which is a function of the nonlinear parameter of the modified Blatz model (see [37]), γ, and the invariants of the Cauchy Green tensor, is introduced to improve the estimation of the nonlinear parameter. The rest of the thesis is organized as following:

Chapter II reviews the theory and finite element formulation of the nonlinear elasticity forward problem for incompressible materials. Specifically, details of Newton's method to solve nonlinear equations due to geometric and material nonlinearity, and stabilization techniques to handle incompressibility are discussed. Then the inverse problem formulation is introduced with a brief description of the adjoint equations and the optimization scheme used.

Chapter III introduces a new approach to improve the estimation of the nonlinear parameter γ in the modified Blatz model for plane strain incompressible problems. To this

end, a new parameter, β, is defined and the methodology and the steps in obtaining the solution to the inverse problem w.r.t this parameter are discussed.

Chapter IV compares results obtained from the new approach to results from the previous methods. Different inclusion geometries and boundary conditions are tested and analyzed for improvement in the estimation of the nonlinear parameter.

Chapter V concludes the thesis with a summary, drawbacks, and future work.

CHAPTER II

THEORY OF NONLINEAR ELASTICITY AND INVERSE PROBLEMS

In the context of biological soft tissues which exhibit highly nonlinear behavior the inverse problem becomes complicated and the solution method needs to be more sophisticated in order to achieve accuracy. In this chapter a description of the general nonlinear elasticity problem and the corresponding inverse formulation as derived in [37] is reviewed. A particular hyperelastic model namely the modified Blatz model for an incompressible material is discussed in detail under the plane strain assumption and the corresponding formulations are shown.

This chapter is organized into 2 sections. The first section describes the forward problem in nonlinear elasticity and the finite element formulation for the same with stabilization terms required for an incompressible material modeled in plane strain. The second section formulates the inverse problem in terms of a cost function and a regularization term. A description of the minimization scheme and the gradient calculation by the adjoint equations is also included.

2.1 Forward Problem in Nonlinear Elasticity

The forward problem in elasticity refers to the boundary value problem that needs to be solved in order to predict the mechanical response of a material given the material properties. The boundary value problem for any material is written in terms of the equilibrium equations and the boundary conditions as follows. (All equations are written in the Lagrangian frame)

$$\nabla \cdot (\boldsymbol{FS}) = 0 \quad in \ \Omega_0 \tag{1}$$

$$\boldsymbol{u} = \boldsymbol{g} \quad on \ \Gamma_g \tag{2}$$

$$\boldsymbol{FS} \cdot \boldsymbol{n} = \boldsymbol{h} \quad on \ \Gamma_h \tag{3}$$

And the constraint due to incompressibility of the material is given by

$$\det(\boldsymbol{F}) - 1 = 0 \quad in \ \Omega_0 \tag{4}$$

where $\boldsymbol{F}$ is the deformation gradient and $\boldsymbol{S}$ is the second Piola-Kirchhoff stress tensor. The Neumann boundary conditions are described by Eq. (3) where $\boldsymbol{h}$ is the prescribed traction on the undeformed boundary Γ_h on which **n** is the unit outward normal. Dirichlet boundary conditions are specified in Eq. (2) in terms of $\boldsymbol{g}$ which are the prescribed displacements on the undeformed boundary Γ_g. The boundaries Γ_h and Γ_g are assumed to satisfy $\partial\Omega_0 = \overline{\Gamma_g \cup \Gamma_h}$ and $\Gamma_g \cap \Gamma_h = \emptyset$ meaning the entire boundary is classified into regions where displacement is specified and regions where traction is specified.

In addition to the equations and constraints given in Eqs.(1)-(4), the constitutive equation of the material is required to solve the boundary value problem. A hyperelastic material is defined by a unique strain energy density function from which the constitutive relation for the material is derived. For a general hyperelastic material of strain energy density $W(\boldsymbol{C})$ which is nonlinear, the second Piola-Kirchhoff stress **S** is given by

$$\boldsymbol{S} = -pJ\boldsymbol{C}^{-1} + 2\frac{\partial W(\boldsymbol{C})}{\partial \boldsymbol{C}} \tag{5}$$

where p is the pressure and J is the Jacobian which is the determinant of the deformation gradient here. Different hyperelastic models have different forms of the function $W(\boldsymbol{C})$ and is usually written in terms of the invariants of **C** which is the right Cauchy-Green deformation tensor.

2.1.1 Weak Formulation for Finite Element Analysis

The weak form for FE analysis of the boundary value problem described in Eqs. (1)-(4) in its strong form can be derived by multiplying Eq. (1) by a vector test function and equating the integral over the reference domain to zero. Then by applying integration-by-parts over the domain and enforcing traction boundary conditions the weak form is obtained. The incompressibility constraint is also enforced in a weak sense by multiplying by another test function and integrating it over the reference domain. The equations of the weak form are given by:

$$\int_{\Omega_0} w_{k,i} F_{kj} S_{ij} d\Omega_0 + \int_{\Omega_0} (J-1) v \, d\Omega_0 - \int_{\Gamma_h} w_i h_i \, d\Gamma_0 = 0 \qquad \textbf{(6)}$$

$$\forall \boldsymbol{W} \equiv [w, v] \in \mathcal{Q} \times \mathcal{P}$$

where the solution of Eq. (6) is solved for displacements and pressure represented by the vector $\boldsymbol{U} \equiv [\boldsymbol{u}, p] \in \mathcal{M} \times \mathcal{P}$.

The functional sub-spaces are defined by

$$\mathcal{Q} = \left\{ \boldsymbol{w} \middle| w_i \in H^1(\Omega_0);\ w_i = 0 \ on \ \Gamma_g \right\} \qquad \textbf{(7)}$$

$$\mathcal{M} = \left\{ \boldsymbol{u} \middle| u_i \in H^1(\Omega_0);\ u_i = g_i \ on \ \Gamma_g \right\} \qquad \textbf{(8)}$$

$$\mathcal{P} \subseteq L_2(\Omega_0) \qquad \textbf{(9)}$$

The weak form in Eq. (6) can be written in the semi-linear form as

$$\mathcal{A}(\boldsymbol{W}, \boldsymbol{U}; \boldsymbol{\psi}) - (\boldsymbol{w}, \boldsymbol{h})_{\Gamma_h} = 0 \qquad \textbf{(10)}$$

where $\mathcal{A}(\boldsymbol{W}, \boldsymbol{U}; \boldsymbol{\psi})$ includes the combination of the first two terms in Eq. (6) and $(\boldsymbol{w}, \boldsymbol{h})_{\Gamma_h}$ represents the surface integral of the traction in the third term. $\boldsymbol{\psi}$ denotes the vector of material parameters for a given hyperelastic model.

The weak form is then discretized which results in a nonlinear system of equations from which the displacement and pressure are to be solved. The nonlinear system of equations can be solved by linearization and using the Newton-Raphson method.

2.1.2 Hyperelastic Models and Strain Energy Density Functions

The hyperelastic models typically used to describe soft tissues produce exponential stiffening with increase in strain [36] – [37]. Specifically, the modified Blatz model that is used in this thesis has a strain energy density function given by

$$W = \frac{\mu}{2\gamma}\left(e^{\gamma\left(J^{-\frac{2}{3}}I_1 - 3\right)} - 1\right) \qquad \textbf{(11)}$$

where μ and γ are the two material parameters of the model. μ is interpreted as the shear modulus at zero strain and γ captures the nonlinearity of the material response at large strains. $I_1 = trace(\boldsymbol{C})$ is the first principal invariant of the Cauchy Green tensor and J being the determinant of the deformation gradient represents the volume change of the material. The shear modulus μ dominates the response of the material at small strains and γ governs the exponential stiffening of the material. The second Piola Kirchhoff stress for this material can be derived in terms of the volumetric and deviatoric part from Eq. (5) and Eq. (11) as

$$\boldsymbol{S} = -pJ\boldsymbol{C}^{-1} + \mu J^{-\frac{2}{3}}\left(\boldsymbol{I} - \frac{1}{3}I_1\boldsymbol{C}^{-1}\right)e^{\gamma\left(J^{-\frac{2}{3}}I_1 - 3\right)} \qquad \textbf{(12)}$$

for which the Cauchy stress is given by

$$\boldsymbol{\sigma} = -p\boldsymbol{I} + \mu J^{-\frac{5}{3}}(\boldsymbol{F}\boldsymbol{F}^{\boldsymbol{T}} - \frac{1}{3}I_1\boldsymbol{I})e^{\gamma\left(J^{-\frac{2}{3}}I_1-3\right)} \quad \textbf{(13)}$$

The hydrostatic pressure is given by $p = -\frac{trace(\sigma)}{3}$. The material tangent tensor for this model can been derived as

$$\mathcal{C}_{ijkl} = 2\frac{\partial S_{ij}}{\partial C_{kl}} = 4\frac{\partial^2 W}{\partial C_{ij}\partial C_{kl}} - 2\frac{\partial}{\partial C_{kl}}\left(pJC_{ij}^{-1}\right)$$

$$\mathcal{C}_{ijkl} = 2\mu e^{\gamma\left(J^{-\frac{2}{3}}I_1-3\right)}\left(\gamma L_{ij}L_{kl} - \frac{1}{3}C_{kl}^{-1}L_{ij} + \mathcal{D}_{ijkl}\right) - p\mathcal{E}_{ijkl} \quad \textbf{(14)}$$

where

$$L_{ij} = J^{-\frac{2}{3}}\left(-\frac{1}{3}I_1C_{ij}^{-1} + \delta_{ij}\right) \quad \textbf{(15)}$$

$$\mathcal{D}_{ijkl} = -\frac{1}{3}J^{-\frac{2}{3}}\left(\delta_{kl}C_{ij}^{-1} - \frac{1}{2}I_1(C_{ik}^{-1}C_{jl}^{-1} + C_{il}^{-1}C_{jk}^{-1})\right) \quad \textbf{(16)}$$

$$\mathcal{E}_{ijkl} = J\left(C_{ij}^{-1}C_{kl}^{-1} - C_{ik}^{-1}C_{jl}^{-1} - C_{il}^{-1}C_{jk}^{-1}\right) \quad \textbf{(17)}$$

2.1.3 Stabilization of the FEM Formulation for Incompressible Materials

Discretization of the weak form given in Eq.(6) using finite dimensional subspaces, followed by linearization for the Newton-Raphson methods leads to a system that does not satisfy the Ladyzhenskaya-Babuska-Brezzi (LBB) conditions (see [41]) when equal order polynomials are used to approximate the displacements and pressure

fields [39]. The linearized system of equations result in a typical saddle point problem which is given by

$$\begin{bmatrix} \boldsymbol{K_{11}} & \boldsymbol{K_{12}} \\ \boldsymbol{K_{21}} & \boldsymbol{0} \end{bmatrix} \begin{Bmatrix} \boldsymbol{u} \\ \boldsymbol{p} \end{Bmatrix} = \{RHS\} \qquad \textbf{(18)}$$

The matrix $\boldsymbol{K_{12}}$ results in spurious oscillations in the pressure fields and locking in the displacement field because it does not satisfy the inf-sup conditions for discrete systems. In the formulation of the forward problem for incompressible materials in this thesis, the stabilized finite element approach based on the streamline upwind (SUPG) method (see [42]) is used. As a result, an additional stabilization term is added to the weak form which stabilizes the equations. The modified set of equations are given by

$$\mathcal{A}(\boldsymbol{W}^h, \boldsymbol{U}^h; \boldsymbol{\psi}) + \mathcal{R}(\boldsymbol{W}^h, \boldsymbol{U}^h; \boldsymbol{\psi}) = (\boldsymbol{w}^h, \boldsymbol{h})_{\Gamma_h} \qquad \textbf{(19)}$$

$$\forall \boldsymbol{W^h} \equiv [w^h, v^h] \in \mathcal{Q}^h \times \mathcal{P}^h$$

where the stabilization term is given by

$$\mathcal{R}(\boldsymbol{W}^h, \boldsymbol{U}^h; \boldsymbol{\psi}) = -\sum_{e=1}^{n_{el}} (\tau \nabla . (\boldsymbol{FS}), \boldsymbol{F}^{-T} \nabla v^h)_{\Omega_0^e} \qquad \textbf{(20)}$$

The solution of Eq.(19) gives the displacements and pressure of the boundary value problem represented by the vector $\boldsymbol{U} \equiv [\boldsymbol{u}, p] \in \mathcal{M} \times \mathcal{P}$.

In Eq. (20), $(.,.)_{\Omega_0^e}$ denotes the $L_2(\Omega_0^e)$ inner product evaluated in the interior of the e^{th} element and

$$\tau = \frac{\alpha h^2}{2\mu} \qquad \textbf{(21)}$$

where τ comprises of a factor $\alpha \approx 1/2$, the shear modulus μ , and h represents the characteristic length of the element which is the diameter of the circumcircle of triangular elements. The stabilization term can be simplified as (see [43])

$$\mathcal{R}(\boldsymbol{W}^h, \boldsymbol{U}^h; \boldsymbol{\psi}) = \sum_{e=1}^{n_{el}} (\tau J \boldsymbol{F}^{-T} \nabla p^h, \boldsymbol{F}^{-T} \nabla v^h)_{\Omega_0^e} \qquad \textbf{(22)}$$

The above stabilization term produces a matrix system which is more stable, prevents solving a saddle point problem and as a result circumvents the LBB condition. The final linearized matrix system is given by

$$\begin{pmatrix} \boldsymbol{K_{11}} & \boldsymbol{K_{12}} \\ \boldsymbol{K_{21}} & \boldsymbol{K_{22}} \end{pmatrix} \begin{pmatrix} u \\ p \end{pmatrix} = (RHS) \qquad \textbf{(23)}$$

where the linearized stiffness matrix is positive definite.

2.2 Inverse Problem Formulation

The inverse problem for incompressible materials has been formulated as an optimization problem as described in [39] and [43] where the material parameters are optimized to fit the measured displacement fields. A regularization term is also added to the optimization problem to reduce noise amplification in the material parameters caused by noise in the displacement measurements. The limited BFGS algorithm [44] is used to solve this optimization problem. This algorithm requires the calculation of gradients of the objective function and this is achieved by the adjoint equations which are briefly described in section **2.2.2** and in detail in [39]. In each iteration a forward problem and an adjoint problem is solved.

2.2.1 Statement of the Inverse Problem

The inverse problem is posed as a constrained minimization problem whose objective function is given by

$$\pi = \frac{1}{2}\sum_{i=1}^{n} w_i \left\| \boldsymbol{T}\boldsymbol{u}^{\boldsymbol{i}} - \boldsymbol{T}\boldsymbol{u}^{\boldsymbol{i}}_{\boldsymbol{meas}} \right\|_0^2 + \frac{1}{2}\sum_{j=1}^{2} \alpha_j R(\psi_j) \qquad \textbf{(24)}$$

where the material properties are $\boldsymbol{\psi} = [\psi_1, \psi_2] = [\mu, \gamma]$. The optimization is constrained such that the computed displacements $\boldsymbol{u}^{\boldsymbol{i}}$ satisfy the equilibrium equations and boundary conditions of the boundary value problem in the weak form. The first term in equation Eq. (24) minimizes the discrepancy in the measured and computed displacement fields where the brackets $\|.\|_0$ denote the L_2 norm. w_i are the weights assigned to each displacement field depending on the magnitude of the displacement. The tensor **T** is a diagonal tensor that assigns weight to each component of the displacement field.

The second term in Eq. (24) is the regularization term which helps alleviate the ill-posed nature of the inverse problem. The regularization parameter α_j depends on the noise level and can be chosen by the L-curve method or Morozov's principle [46]. For analysis in this paper the total variation diminishing (TVD) regularization is used which is defined as

$$R(\psi_j) = \int_{\Omega_0} \sqrt{\left|\nabla\psi_j\right|^2 + c^2}\; d\Omega_0 \qquad \textbf{(25)}$$

where c is a small constant value to ensure smoothness of the regularization term when $\left|\nabla\psi_j\right| = 0$.

2.2.2 Adjoint Equations

The gradients of the objective function defined in equation Eq. (24) have to be evaluated for the discretized problem. The gradient at the discrete level is the vector containing the changes in the value of the objective function for small changes in the material parameter applied one node at a time. This means the most direct way to obtain the gradients would involve solving the forward problem the number of times equal to the number of nodes. A more efficient way in the form of the adjoint equations was first introduced by Oberai et al [16, 17]. Obtaining the gradient of the objective function through the adjoint equations would involve solving the forward problem and an adjoint problem once as compared to solving the forward problem many times as part of the direct calculation of gradients. The details of the equations for a general nonlinear hyperelastic model and are not presented here. The reader is directed to [39, 43] for the derivations of these equations.

A continuation in material properties scheme as described in [43] is used here as well to reduce computational effort in solving the inverse problem. The idea here is to use the converged solution of a previous BFGS iteration of the inverse problem as the initial guess to solve the forward problem in the current iteration by just using one load step instead of many under large deformations.

In this chapter the theory and formulation of the general forward and inverse problems in nonlinear elasticity were reviewed. The purpose of this chapter is to provide the reader with a broad understanding of the concepts needed in order to appreciate the new parameter introduced in the next chapter and the results following that.

CHAPTER III

IMPROVED ESTIMATION OF NONLINEAR BEHAVIOR WITH NEW PARAMETER

The reconstruction of the nonlinear parameter, γ, which characterizes the nonlinear behavior of tissues, in the presence of noisy displacement data is a complicated and challenging problem to solve. It has been shown that cancerous tissues stiffen at a much higher rate than healthy tissues with increasing strain (see [28, 29]). Thus, obtaining accurate estimations of the nonlinearity parameter is crucial to distinguish cancerous from healthy tumors.

In the following subsections, the difficulties and inaccuracies in the previous method to obtain γ at high noise levels in the displacement field are discussed.

3.1 Measures of Nonlinearity

3.1.1 Previous Method of Estimating γ

Studies about the reconstruction of the two material properties of the modified Blatz model, namely the shear modulus μ and the nonlinear parameter γ, for numerical experiments and for experimental data have been published. The following observations are made regarding the existing direct approach taken to reconstruct the desired parameters.

For inverse reconstructions involving only displacement boundary conditions, the inhomogeneous shear modulus μ can be recovered only up to a multiplicative constant. This can be shown from the equilibrium equation defined in Eq. (1). Due to the particular form of total variation diminishing(TVD) regularization, the regions of lower μ, i.e. softer

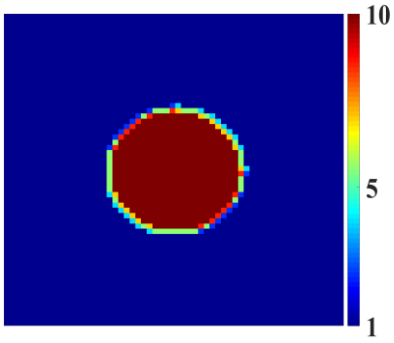

Figure 1. Target γ (comparison)

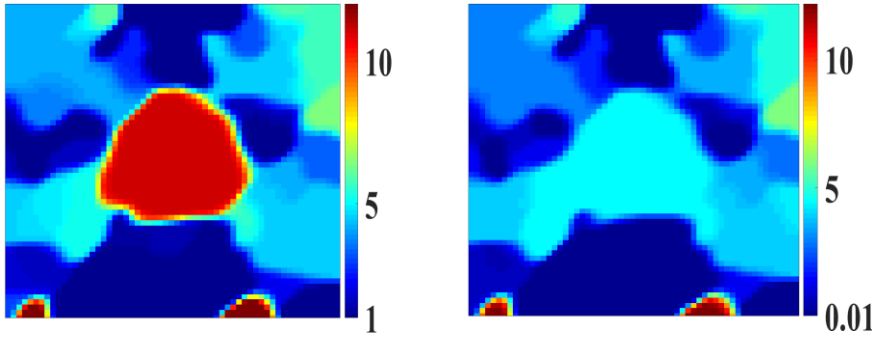

Figure 2. (a) Reconstructed γ – Lower Bound 1, (b) Reconstructed γ – Lower Bound 0.01

regions, are driven to the lower bound specified for the minimization problem. In the case of a stiff inclusion in a soft background, the region outside the inclusion are driven to the lower bound. However, the ratio of the shear modulus of inclusion to background is still preserved. This property is very useful and can be used effectively to obtain accurate relative inclusion contrast.

However, the reconstruction of the nonlinear parameter γ is not as simple or well behaved as that of the shear modulus. It has been observed that the lower bound used in the optimization process significantly affects the solution obtained but with no contrast

preservation. In the presence of displacement noise levels close to 3%, which is commonly observed in actual ultrasound measurements, the solution to the inverse problem (γ distribution) has been found to be highly sensitive to the region of search for the solution. The results vary significantly for different lower bounds as shown in Figure 2. The reconstructions reported in [37] at high nonlinearities (meaning large enough strain to observe significant nonlinearity) are well recovered owing to the reason that the lower bound is close to the target value of γ in the background. However, when the problem was attempted to be solved with a lower bound smaller than the target, it was observed the reconstructions reduced in quality in terms of shape and contrast and in some cases the nonlinear signal was not even observable. This is a major issue because in actual tissues, e.g., breast tissues, the background value of γ is not known, that might lead to poor reconstructions, resulting in biased interpretation of tissue pathology.

The stress-strain relationship in 3D defined in Eq. (13) can be expressed for uniaxial loading with stretch λ as

$$\sigma = \mu\left(\lambda^2 - \frac{1}{\lambda}\right) e^{\gamma\left(\lambda^2+\frac{2}{\lambda}-3\right)} \qquad \textbf{(26)}$$

From the uniaxial stress stretch plot shown in Figure 3, one can observe that at low stretch values the curves corresponding to different γ values are very close to each other and will be indistinguishable in the presence of dominating noise. A minimum strain required to capture the nonlinear signal can thus be calculated to distinguish between γ values [36]. From Figure 3 the minimum strain also depends on the contrast of γ in the problem. Smaller contrasts require higher strains and larger contrasts require smaller

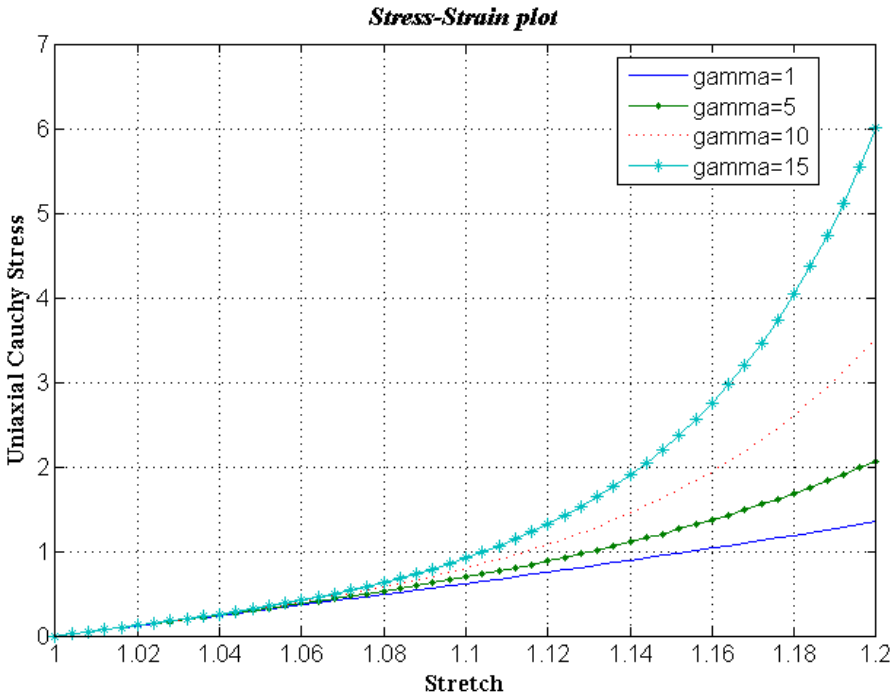

Figure 3. Uniaxial Stress-stretch plot for different values of γ and a constant shear modulus value of 1, (Ref. [43])

strains for a good reconstruction when there is noise in the displacement data. Considering the issues outlined above for the previous method of recovering the nonlinearity parameter γ, a new method is sought.

3.1.2 Definition of a New Parameter for Nonlinear Behavior

The shear modulus reconstruction has the advantage of preserving the relative contrast as described before. It is understood that relative contrast reconstructions of the shear modulus work very well with the regularizations utilized in this thesis. Thus, we attempt to make use of this observation to introduce a new parameter that improves the nonlinear parameter reconstruction. In the strain energy density function of the modified

Blatz model defined in Eq. (12), the shear modulus, μ , and the exponential term appear as a product. So the idea is to define a new parameter, β, that combines them, as

$$\beta = e^{\gamma(I_1-3)} \quad \textbf{(27)}$$

which will lead to the definition of the second Piola Kirchhoff stress as

$$\boldsymbol{S} = -pJ\boldsymbol{C}^{-1} + \mu\,\beta J^{-\frac{2}{3}}(\boldsymbol{I} - \frac{1}{3}I_1\boldsymbol{C}^{-1}) \quad \textbf{(28)}$$

and the material tangent becomes

$$\mathcal{C}_{ijkl} = 2\mu\beta\left(-\frac{1}{3}C_{kl}^{-1}L_{ij} + \mathcal{D}_{ijkl}\right) - p\mathcal{E}_{ijkl} \quad \textbf{(29)}$$

with the tensors in the above equation defined in Eqs. (15)-(17). It is noted that for the modified Blatz model studied here, the desired properties of the shear modulus can be obtained with β. This is because both parameters occupy an indistinguishable position in Eq. (28).

The range of values that β can take depends on the range of γ and $I_1 - 3$. For incompressible materials one can show that $I_1 - 3$ is always greater than 0. And from thermodynamic constraints on the hyperelastic Blatz model, γ is also always greater than 0. From this, one can deduce that β is always greater than 1. Under a given stress state, γ and $I_1 - 3$ act in an opposing fashion, i.e. higher the value of γ at a certain region lower the strain experienced in that region and vice-versa. It is important to note that the new parameter, β, is not an actual material property based on the model but rather a convenient parameter devised to make computations in the inverse problem simpler and possibly more accurate.

Now that the new parameter is introduced, we look at how the inverse problem is solved for β. In accordance with the introduction of β, the corresponding nonlinear finite element equations are modified. With the input of measured displacement data, obtained from numerical or physical experiments, the inverse problem is solved for the β distribution by minimizing the discrepancy in the measured and computed displacements. Suitably modified adjoint equations are used for the calculation of gradients and a TVD regularization scheme is implemented. It is straight forward to express the adjoint equations for this model and is omitted here. Finally, the regularization term given in Eq. (25) will be used for the reconstruction of the new parameter, β .

3.2 Estimation of Nonlinear Behavior with New Parameter

3.2.1 Post Processing of β to Obtain γ

The parameter β in itself may not have a direct physical meaning with regard to the nonlinear behavior of the material, but it serves as an intermediate parameter to obtain the nonlinear parameter γ accurately which in turn characterizes the nonlinear behavior of the material. Therefore, once the reconstruction of β is obtained by solving the inverse problem, post processing is needed to obtain the distribution of the "actual" nonlinear parameter, γ, of the modified Blatz model. The computed displacement field in the objective function, under the constraint of the forward elasticity problem, is utilized after the inverse problem converges to calculate γ from β. This computed displacement field results in a strain field and invariants that are significantly smoother than that from the measured displacement field. Eq. (27) can be rewritten to obtain γ as

$$\gamma = \frac{\ln(\beta)}{I_1 - 3} \quad \textbf{(30)}$$

where the value of the first invariant, I_1, of the Cauchy Green Tensor, $\boldsymbol{C}$, is calculated from the computed displacement field.

3.2.2 Uniqueness of β and μ Using Dirichlet Boundary Conditions

When the problem of interest consists of boundary conditions only in the form of prescribed displacements, from Eq. (28) it can be deduced that values of β and μ can be determined only up to a multiplicative factor. This idea has been discussed in detail for the shear modulus μ and the pressure p (see [43]). When the term $\mu\beta$ in Eq. (28) is chosen as $\mu(\boldsymbol{x})\beta(\boldsymbol{x}) = \beta_0\mu(\boldsymbol{x})\beta_r(\boldsymbol{x})$ and the pressure is chosen as $p(\boldsymbol{x}) = p_0 + p_r(\boldsymbol{x})$, where β_0 and p_0 are constants, the equilibrium equation Eq. (1) would be satisfied for any values of β_0 and p_0. $p_r(\boldsymbol{x})$ and $\beta_r(\boldsymbol{x})$ are the values of as p and β obtained as solutions from the inverse problem.

In [43] it is argued that in the presence of zero normal traction conditions the value of p_0 is zero. So when using only displacement boundaries, it is important to take care of the calibration of μ and β from the inverse problem solution. This is especially relevant in terms of application of this method in identification of tumors in biological tissues using ultrasound techniques. These parameters could potentially be calibrated using an overall measured force and the solution of γ distribution is obtained from Eq. (30). The calibration of the parameter β is needed when only Dirichlet boundary conditions are specified to estimate the multiplicative constant, β_0. Let β and β_r be defined by Eq. (27) with γ and γ_r respectively, and $\beta = \beta_0\beta_r$, then

$$e^{\gamma(I_1-3)} = e^{(\gamma_0(I_1-3)+\gamma_r(I_1-3))}$$

$$\gamma = \gamma_0 + \gamma_r \quad \textbf{(31)}$$

where

$$\gamma_0(\boldsymbol{x}) = \frac{\ln(\beta_0)}{I_1(\boldsymbol{x}) - 3} \quad \textbf{(32)}$$

The value of β_0 can be found from the equation of force at the boundary which is given in terms of the stress from Eq. (3) by

$$T = \int_{\Gamma_h} \boldsymbol{FS} \cdot \boldsymbol{n}\, dA \quad \textbf{(33)}$$

where S is a function of β_0 and β_r, as seen from Eq. (28), and T is the total force at the boundary Γ_h.

Thus it is shown that, before calibration, the calculation of γ is off by an additional term γ_0 which is a function of the first invariant of strain and so is not necessarily a constant over the domain. This creates a difficulty especially when the inverse problem is solved for γ directly. Eq. (32) shows that calibration for γ is not straight forward as the calibration factor γ_0 is a function of the strain, $I_1(\boldsymbol{x}) - 3$, which varies in space. However, it is much simpler to calibrate for β. Results from both methods are presented and compared in Chapter IV.

CHAPTER IV

NUMERICAL EXPERIMENTS

In this chapter results, comparison and discussion of different numerical experiments based on the methods described in Chapter III are presented. It is organized into two major sections corresponding to two different inclusion geometries in 2D. In each section the results from the previous and new methods are compared. In the numerical experiments, measured displacement data is simulated by obtaining the displacement field based on a known target distribution of μ and γ and then adding random white noise. This is then fed as input to the inverse solver to recover the known target distributions. The displacement data is added with noise to emulate experimental observations obtained from ultrasound devices. The parameters μ and γ can either be obtained simultaneously or in sequence with two different displacement fields [43]. Because of the dependability of the parameter β on the strain, $I_1 - 3$, its distribution varies depending on the loading. So in all reconstructions in this thesis, the sequence approach is followed where the shear modulus distribution is first separately reconstructed with a smaller loading. The material parameter reconstructions obtained by solving the inverse problem by both methods are presented in this chapter along with discussions.

4.1 One Big Inclusion

A target material distribution corresponding to a large stiff inclusion at the center of the domain is studied first. Here two sub-problems are considered- one with a higher shear modulus and higher γ in the inclusion and the other one with a uniform shear

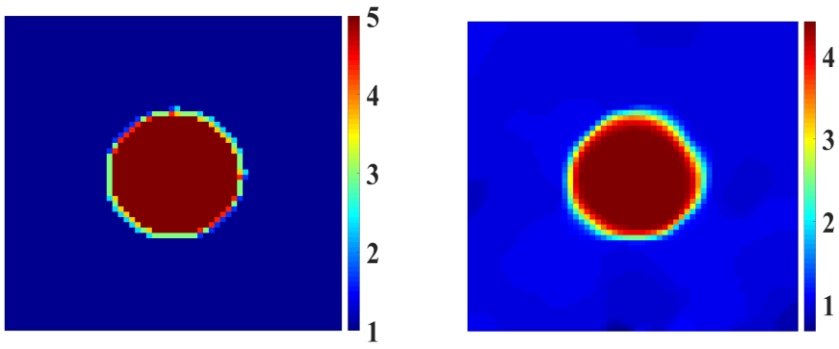

Figure 4. (a) Target μ, (b) Reconstructed μ (3% noise)

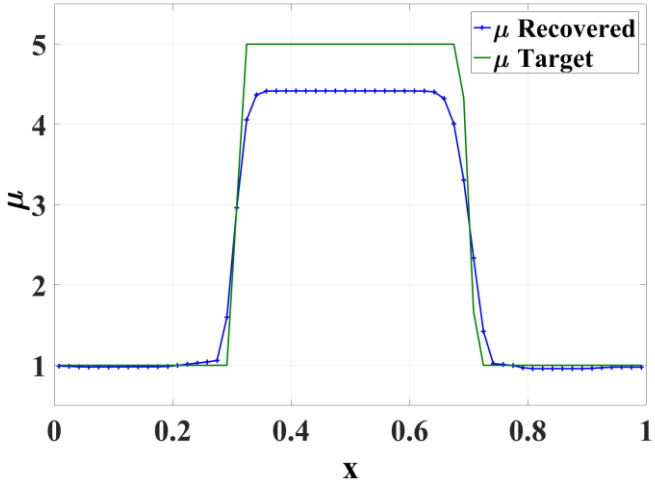

Figure 5. Horizontal Centerline plot of the Shear Modulus

modulus distribution but higher γ in the inclusion. The following sections contain results and discussion for the two sub-problems.

4.1.1 Inclusion with Contrast in Both γ and μ

The target distributions for μ and γ are shown in Figure 4&7, where one inclusion of diameter 40% the size of the domain, is located at the center. Two separate loadings of compressive traction are applied as boundary conditions on the top surface, while the sides

are subjected to zero traction and the bottom surface is fixed in the direction of loading while allowed to slide freely in the lateral direction. The first smaller loading is of magnitude 0.05 and second larger loading is 0.6. The center of the bottom surface is fixed both axially and laterally to avoid rigid body motion causing instability in the FEM solution. The unit square domain shown in the figure is subjected to a uniform traction compressive loading on the top. The system is solved by discretizing the domain into a mesh of 7200 triangular elements. The measured displacement data is obtained for each loading by solving the forward problem for the target distribution shown in Figure 7, and adding Gaussian white noise of magnitude 3% to the displacement in the direction of loading. The inverse problem is then solved by matching the displacements in the axial direction.

The reconstruction of the shear modulus can be obtained by ignoring the effect of the nonlinear parameter for the smaller loading because the deformations are small. This reconstructed shear modulus distribution, shown in Figure 4(b)&5, is then fixed in order to obtain the reconstructions of the nonlinear parameter, γ and the new parameter β using the larger loading.

Traction Controlled Loading

In the first sub-case, the boundary conditions or loading on the top surface of the domain are prescribed in terms of traction. The reconstruction of β for the larger loading condition is given in Figure 7(a). Suitable values are chosen for the regularization parameter, α, described in Eq. (24). The corresponding γ distribution calculated during post processing is shown in Figure 6&7(b).

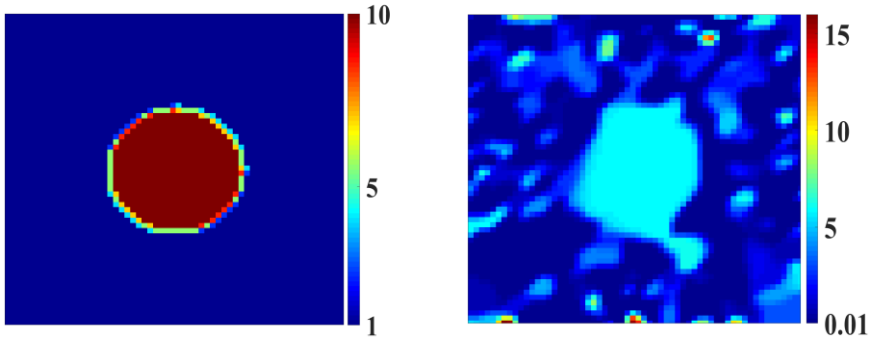

Figure 6. *Traction Controlled*: (a) Target γ distribution, (b) γ reconstruction from direct optimization with lower bound 0.01

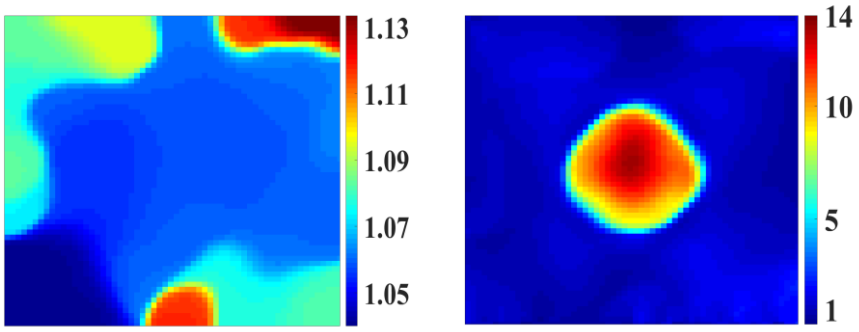

Figure 7. *Traction Controlled*: (a) β reconstruction, (b) γ reconstruction from β by post-processing

The lower bound used for the reconstruction of β is 1.01 and the upper bound is 5. These bounds were chosen to approximately be equivalent to a lower bound of 0.01 and an upper bound of 30 in the direct optimization problem for γ. The reconstruction of γ from the direct optimization of γ, which is the previously existing method, is given in Figure 7(b). The superior performance of reconstruction using the new parameter is easily seen from Figure 6&7(b).

The quality of the reconstruction of γ is compromised in terms of the shape of the recovered inclusion and the contrast in the previous method. The new method produces

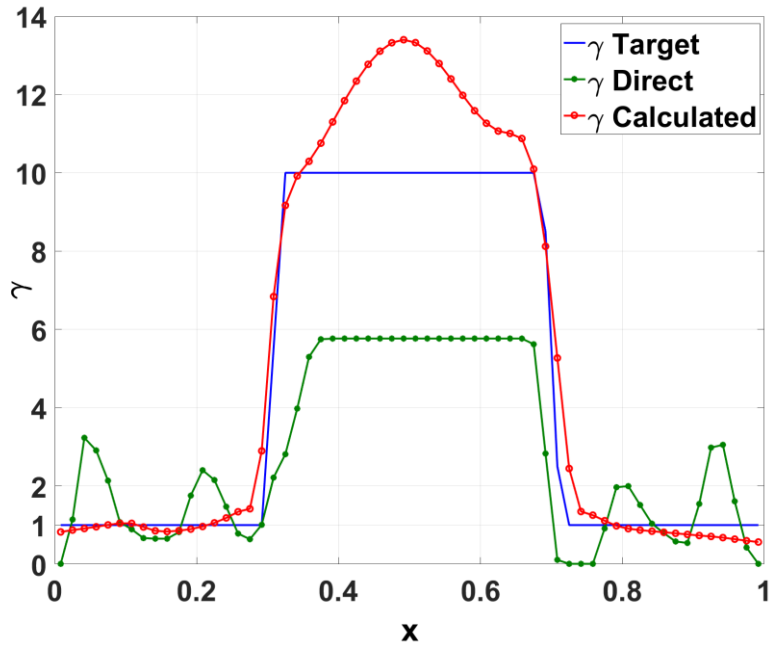

Figure 8. *Traction Controlled* : Horizontal Centerline plot of γ obtained from the two methods compared with the target

good reconstructions at medium strains which the previous method is shown to fail in the presence of noise. This is because of less pronounced nonlinearity at medium strains as discussed in section 3.1.1 and illustrated in Figure 3. When the applied load is not sufficiently large to invoke strong nonlinearity or when the nonlinearity is not strong enough (low γ), noise in the displacement data can result in poor contrast of inclusion versus background. This has been discussed in [36] and a rough estimate of the relationship between the noise level and the applied strain has been derived. However, this estimate does not address the fact that the effect of the noise level also depends on the mesh size chosen and so we conclude that this estimate is not very robust. In this example, the magnitude of the traction loading is controlled in such a way as to induce medium strains (around 10%) in order to showcase the effectiveness of the new parameter.

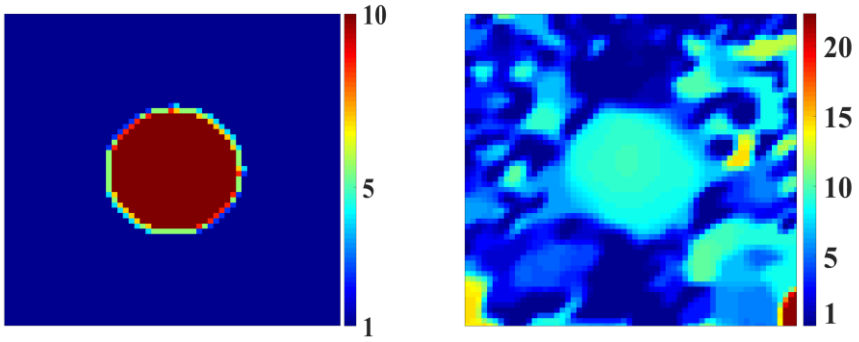

Figure 9. *Dirichlet BC:* (a) Target γ distribution, (b) γ reconstruction from direct optimization with lower bound 0.01

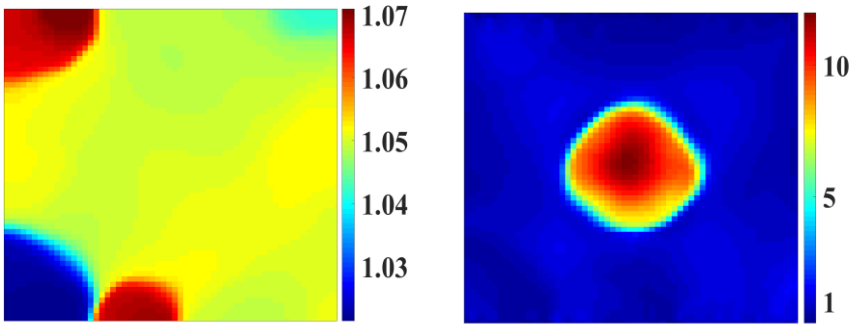

Figure 10. *Dirichlet BC:* (a) β reconstruction, (b) γ reconstruction from β by post-processing

Dirichlet Boundary Conditions

For the purpose of comparison, the same loading considered in the previous section is applied in terms of specified displacements on the top surface instead of uniform traction. The displacement response at the top surface is obtained from the forward problem of a uniform traction loading and prescribed as boundary conditions on the top surface for the inverse problem. It is to be noted that both problems are physically equivalent. It is the method of enforcing boundary conditions that differs. Since most

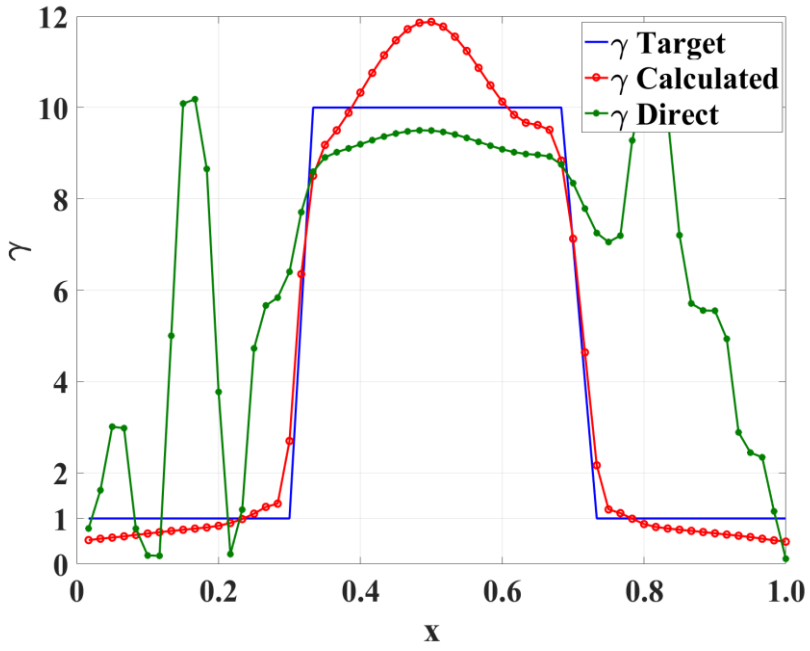

Figure 11. *Dirichlet BC:* Horizontal Centerline plot of γ obtained from the two methods compared with the target

ultrasound devices measure displacements at the boundaries and the interior of the specimen, the behavior of the new method under displacement boundary conditions is studied.

The β reconstruction for this case is shown in Figure 10(a) and the corresponding γ that is calculated during post-processing is shown in Figure 10(b). In the new method, the quality of recovered γ distribution is better in terms of shape definition and contrast of the inclusion than the previous method as can be seen from Figures 9(b)&10(b). The recovered γ distribution from the new method follows similar patterns in distribution in both cases considered because the strain distribution is the same as they are the same problem physically. However, as discussed in section 3.2.3, when only displacements are specified at the boundaries the reconstruction of β is accurate only up to a multiplicative

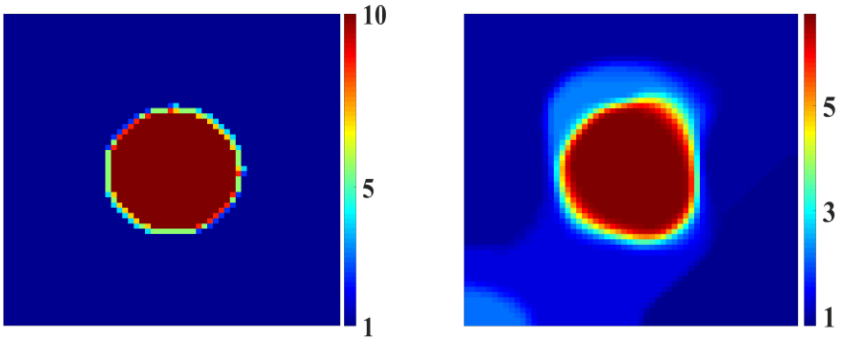

Figure 12. *Uniform μ:* (a) Target γ distribution, (b) γ reconstruction from direct optimization with lower bound 0.01

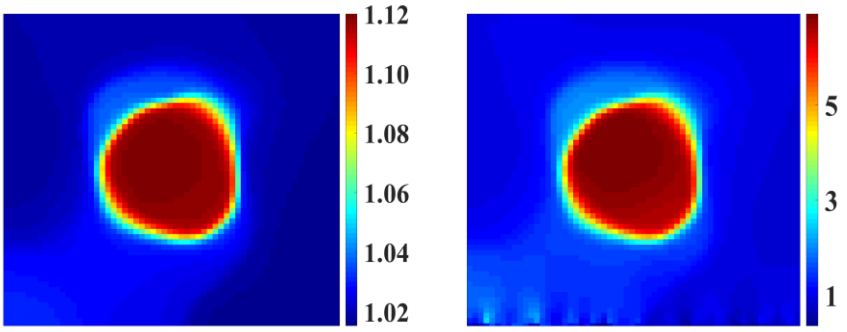

Figure 13. *Uniform μ:* (a) β reconstruction, (b) γ reconstruction from β by post-processing for displacement B.C.

constant. The figures shown for reconstructed γ distribution are obtained after calibrating the solution of β with a multiplicative constant, β_0, which is calculated from the total force on the top surface. In this example, β_0 was calculated to be 1.011 and γ_0 was found from β_0 by Eq. (32) and calibrated according to Eq. (31).

4.1.2 Inclusion with Contrast Only in γ

The target distribution considered in this example has an inclusion with contrast in γ as shown in Figure 6(a), but has a uniform μ. A compressive traction loading of 0.3

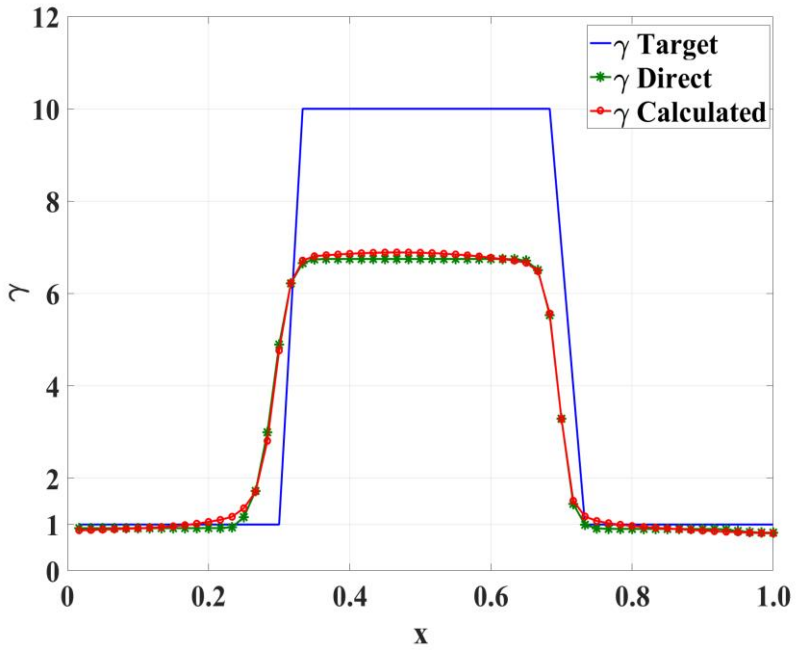

Figure 14. *Uniform μ:* Horizontal Centerline plot of γ obtained from the two methods compared with the target

units is applied on the top surface for this case. A sequential process is followed where the nonlinear parameters are solved by fixing the shear modulus distribution which is uniform in this case. The bounds on the values of β and γ are the same as used in the previous cases. The β distribution is shown in Figure 12(a) and the final solutions of γ from both methods are shown in Figures 12(b)&13(b). As seen from the plots, the solutions obtained from both methods match closely and so it is shown that the new method is as good as the previous method, if not better, in an extreme case of uniform μ. The reason behind considering this case is to show that the β method is able to handle distributions where there is no contrast in strain arising from the presence of a shear modulus, μ. It is important to demonstrate this example where γ is a dominating component in the β distribution,

whereas in the previous example the effect of the contrast in the invariant of strain, $I_1 - 3$, induced by μ and γ were equal but in an opposing sense.

It is worth noting that a clear inclusion in the β distribution is seen in this example because $I_1 - 3$ is more uniform compared to the previous examples. This can be explained by looking at the definition of β in Eq. (34) which is the exponential of the product of $I_1 - 3$ and γ. For any given loading these two quantities are inversely related, i.e. higher the value of γ, lower the deformation (i.e. $I_1 - 3$) and vice-versa. So in the previous examples the contrast in μ created an inverse contrast in $I_1 - 3$ and so its product with γ, i.e. β, was pretty uniformly distributed. The previous method provides reasonably good results in this particular example possibly because the strain is sufficiently large due to a uniform μ.

These two problems successfully show the counteracting effects of γ and $I_1 - 3$ on β as can be seen from Figures 7(a) & 13(a). The new method is able to extract the right contrast in γ in both problems. The effect of the type of boundary conditions and different shear modulus distributions have been shown in this section. However, the effect of the size and multiple inclusions have to be studied. This is discussed in the next section.

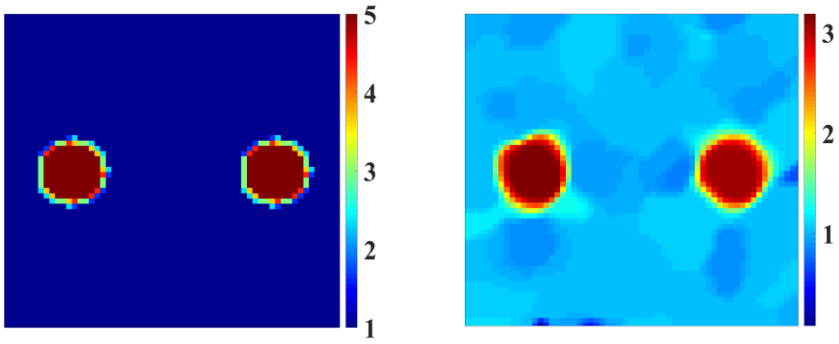

Figure 15. ***Multiple Inclusions:*** **(a) Target μ, (b) Reconstructed μ (3% noise)**

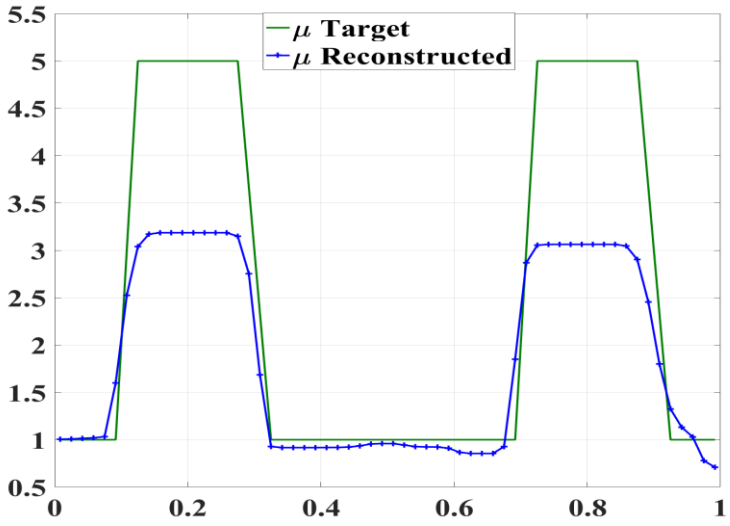

Figure 16. ***Multiple Inclusions*****: Horizontal Centerline plot of the shear modulus**

4.2 Multiple Smaller Inclusions

In this section, the performance of the new method for a case with multiple small inclusions of varying μ and γ is demonstrated. The target shear modulus distribution is shown in Figure 15(a) and the target distribution of γ is shown in Figure 17(a), where 3 small inclusions of varying γ values are shown. The diameter of each inclusion is about 20% of the domain. The value of γ is 1 in the background, 5 in the left most inclusion, 10

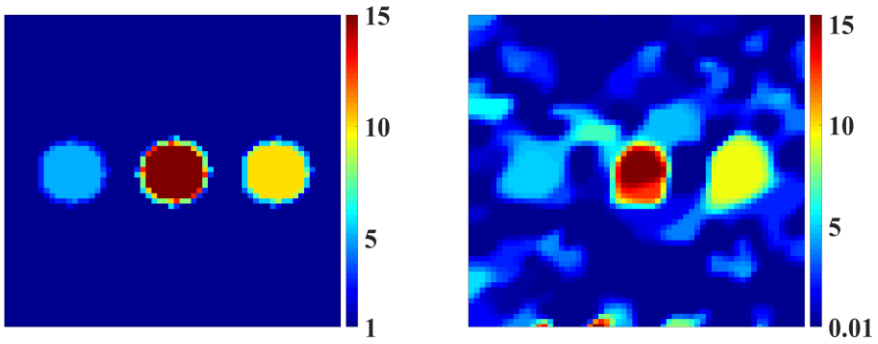

Figure 17. *Multiple Inclusions*: (a) γ target distribution (for comparison), (b) γ reconstruction from direct optimization with lower bound 0.01

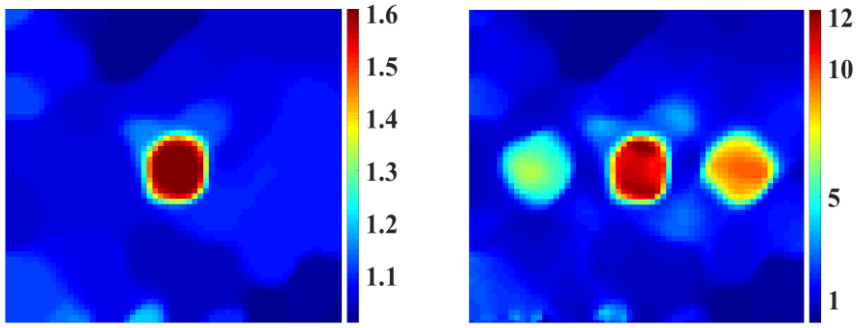

Figure 18. *Multiple Inclusions*: (a) β reconstruction, (b) γ reconstruction from β by post-processing

in the right most inclusion and 15 in the center inclusion. This target distribution is chosen to show the effectiveness of the new method for various inclusions. Uniform traction loading conditions of magnitudes specified in section 4.1.1, i.e. 0.05 and 0.6, are applied on the top surface and 3% Gaussian noise is added to the displacement field in the direction of loading. The boundary conditions for the other sides of the domain are the same as in the previous examples. The reconstructed shear modulus distribution and the comparison with the target distribution are shown in Figure 16. For the larger loading producing

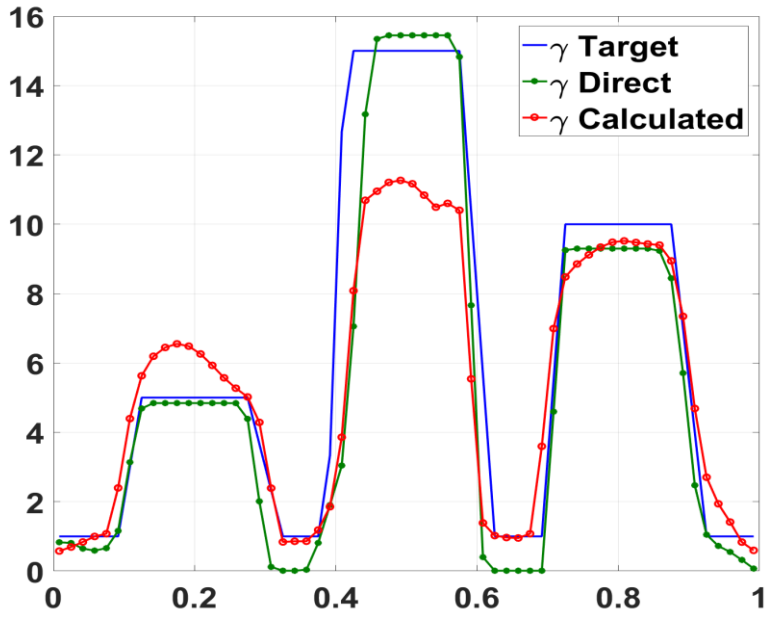

Figure 19. *Multiple Inclusions*: Horizontal centerline plot of γ obtained from the two methods compared with the target

approximately 10% strain at the top, the effect of γ is considerable and is therefore used for reconstructing its distribution.

Comparing the reconstruction of γ from both methods, there is a significant difference in the quality of reconstruction. The new method produces better inclusion shapes than the previous method. Though, from Figure 19 it seems like the contrast is better achieved from the previous method, a closer look at Figure 17(b) will reveal that the uniformity of γ inside the middle inclusion is compromised. There is also significantly less noise in the background for the image produced from the new method.

The low values of γ in the left and right inclusions and the presence of larger μ in the same locations (therefore low strain in the inclusions), results in low nonlinear response in those locations. This leads to poor reconstruction by the previous method in

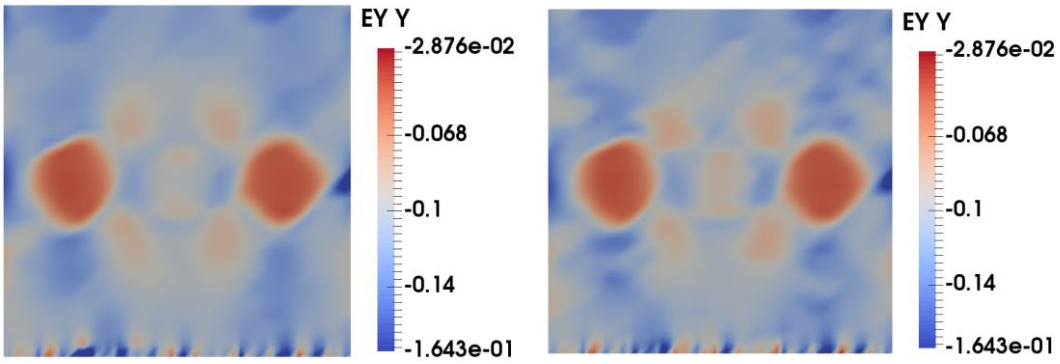

Figure 20: (a) Axial strain from new method, (b) Axial strain from previous method

the presence of noise because of reasons discussed in section 3.1.1. However, β, which is a combination of γ and $I_1 - 3$, is shown to handle noisy displacements better and produces solutions of higher quality overall.

4.3 Discussion

The superior performance of the new method has been demonstrated for various examples. A qualitative explanation for this may be seen by noticing the regularization term in Eqs. (24)&(25). The total variation diminishing regularization term includes the spatial gradient of the solution which results in an overall smoothening of the parameter reconstructed. When the regularization parameter is appropriately chosen, the contrast in the distribution is recovered while overall the solution is smoothened. The regularization parameter serves as the weight for the spatial gradient and so choosing a high value can result in loss of contrast between the inclusion and the background while compromising on matching the measured displacement field. In the previous method, the regularization term caused a smoothness in γ which resulted in a smooth computed displacement field obtained from solving the forward problem.

However, in the new method the regularization term contains $\nabla\beta$ instead of $\nabla\gamma$. From the definition of β in Eq. (27), one can derive

$$\frac{\nabla\beta}{\beta} = \frac{\gamma}{I_1 - 3}\left(\frac{\nabla\gamma}{\gamma} + \frac{\nabla(I_1 - 3)}{I_1 - 3}\right) \quad \textbf{(34)}$$

As the objective function is minimized the regularization term reduces $\nabla\beta$ which results in reduction of both $\nabla\gamma$ and $\nabla(I_1 - 3)$ as shown in Eq. (34). In addition to smoothening in displacement caused by a smooth γ, there is also an indirect smoothening of the computed displacements because of reduction in $\nabla(I_1 - 3)$. In the new method the computed displacement fields can be expected to be smoother and this is seen in Figure 20. The axial strain plots for the two methods are shown for the multiple inclusions example. For both methods, the regularization parameter was chosen carefully in order to maintain contrast while achieving maximum smoothening. Though, it is possible to achieve the same level of axial strain smoothening with the previous method by using a higher regularization parameter, it would result in significant loss of contrast in the inclusion. The new method is able to smoothen the computed displacement field more while still maintaining the contrast of γ in the inclusion. It certainly helps that the post-process calculation of γ in the new method is performed using a smooth displacement field.

Moreover, by introducing β, the nonlinearity arising due to an exponential of the strain is conveniently removed. Post process calculation of γ from β is done using the smooth strains that are obtained after convergence of the inverse problem. Thus, a higher level of smoothness in γ can be expected.

CHAPTER V

CONCLUSION

A new improvised method of obtaining distribution of parameters describing nonlinearity of heterogeneous soft tissues was proposed. The proposed method introduced a new parameter, β, for computational convenience, that reduced the degree of nonlinearity in the hyperelastic modified Blatz model used to describe the mechanical properties of soft tissues. Quality of reconstructions in terms of shape, contrast and background noise were assessed for the new method and compared with the existing method. It was demonstrated that the new method outperforms the previous method when the displacement field is polluted with considerable amount of random noise, through a variety of examples with different boundary conditions and target material parameter distributions. A qualitative reasoning was provided to explain the superior performance of the new method in terms of the degree of smoothness of the computed displacement field in both methods.

The most significant drawback of the new method is that only one displacement field can be used for the inverse reconstructions. That is, multiple loading conditions and the corresponding responses cannot be used simultaneously as that would result in different β distributions for each loading. Multiple loading conditions increase information about the material and therefore typically result in better quality of solutions with the previous method. This also implies that μ and γ cannot be obtained simultaneously in the new method. Some other drawbacks include lack of physical

meaning of β, the need for additional post-processing to obtain γ and restriction of application to a specific hyperelastic model for soft tissues in plane strain.

In conclusion, the new method serves as an improvised tool in determining the nonlinear parameters of soft tissues and provides encouragement to develop similar tools for efficient and accurate determination of nonlinear properties of soft tissues. The most notable application of these techniques is in medicine where, like mentioned before, healthy and cancerous tissues can be differentiated based on stiffness (μ) and rate of stiffening (γ) with strain. (see [10], [40]).

REFERENCES

[1] Ophir, J., Cespedes, I., Ponnekanti, H., Yazdi, Y., & Li, X. (1991). Elastography: a quantitative method for imaging the elasticity of biological tissues. *Ultrasonic Imaging*, *13*(2), 111-134.

[2] Cespedes, I., Ophir, J., Ponnekanti, H., & Maklad, N. (1993). Elastography: elasticity imaging using ultrasound with application to muscle and breast in vivo. *Ultrasonic Imaging*, *15*(2), 73-88.

[3] O'Donnell, M., Skovoroda, A. R., Shapo, B. M., & Emelianov, S. Y. (1994). Internal displacement and strain imaging using ultrasonic speckle tracking. *IEEE Transactions on Ultrasonics Ferroelectrics and Frequency Control*,*41*(3), 314-325.

[4] Pellot-Barakat, C., Frouin, F., Insana, M. F., & Herment, A. (2004). Ultrasound elastography based on multiscale estimations of regularized displacement fields. *Medical Imaging, IEEE Transactions on*, *23*(2), 153-163.

[5] Varghese, T., & Ophir, J. (1997). A theoretical framework for performance characterization of elastography: The strain filter. *Ultrasonics, Ferroelectrics, and Frequency Control, IEEE Transactions on*, *44*(1), 164-172.

[6] Skovoroda, A. R., Emelianov, S. Y., & O'Donnell, M. (1995). Tissue elasticity reconstruction based on ultrasonic displacement and strain images. *Ultrasonics, Ferroelectrics, and Frequency Control, IEEE Transactions on*, *42*(4), 747-765.

[7] Fowlkes, J. B., Emelianov, S. Y., Pipe, J. G., Skovoroda, A. R., Carson, P. L., Adler, R. S., & Sarvazyan, A. P. (1995). Magnetic-resonance imaging techniques for detection of elasticity variation. *Medical Physics*, *22*(11), 1771-1778.

[8] Raghavan, K. R., & Yagle, A. E. (1994). Forward and inverse problems in elasticity imaging of soft tissues. *Nuclear Science, IEEE Transactions on*,*41*(4), 1639-1648.

[9] Sumi, C., Suzuki, A., & Nakayama, K. (1995). Estimation of shear modulus distribution in soft tissue from strain distribution. *Biomedical Engineering, IEEE Transactions on*, *42*(2), 193-202.

[10] Plewes, D. B., Bishop, J., Samani, A., & Sciarretta, J. (2000). Visualization and quantification of breast cancer biomechanical properties with magnetic resonance elastography. *Physics in Medicine and Biology*, *45*(6), 1591.

[11] Bishop, J., Samani, A., Sciarretta, J., & Plewes, D. B. (2000). Two-dimensional MR elastography with linear inversion reconstruction: methodology and noise analysis. *Physics in Medicine and Biology*, *45*(8), 2081.

[12] Kallel, F., & Bertrand, M. (1996). Tissue elasticity reconstruction using linear perturbation method. *Medical Imaging, IEEE Transactions on*, *15*(3), 299-313.

[13] Van Houten, E. E. W., Paulsen, K. D., Miga, M. I., Kennedy, F. E., & Weaver, J. B. (1999). An overlapping subzone technique for MR-based elastic property reconstruction. *Magnetic Resonance in Medicine*, *42*(4), 779-786.

[14] Doyley, M. M., Meaney, P. M., & Bamber, J. C. (2000). Evaluation of an iterative reconstruction method for quantitative elastography. *Physics in Medicine and Biology*, *45*(6), 1521.

[15] Fu, Y. B., Chui, C. K., Teo, C. L., & Kobayashi, E. (2015). Elasticity imaging of biological soft tissue using a combined finite element and non-linear optimization method. *Inverse Problems in Science and Engineering*, *23*(2), 179-196.

[16] Oberai, A. A., Gokhale, N. H., & Feijóo, G. R. (2003). Solution of inverse problems in elasticity imaging using the adjoint method. *Inverse Problems*, *19*(2), 297.

[17] Oberai, A. A., Gokhale, N. H., Doyley, M. M., & Bamber, J. C. (2004). Evaluation of the adjoint equation based algorithm for elasticity imaging. *Physics in Medicine and Biology*, *49*(13), 2955.

[18] Babaniyi, O. A., Oberai, A. A., & Barbone, P. E. (2015). Recovering vector displacement estimates in quasistatic elastography using sparse relaxation of the momentum equation. *arXiv preprint arXiv:1506.04765*.

[19] Geymonat, G., Hild, F., & Pagano, S. (2002). Identification of elastic parameters by displacement field measurement. *Comptes Rendus Mecanique*, *330*(6), 403-408.

[20] Florentin, E., & Lubineau, G. (2010). Identification of the parameters of an elastic material model using the constitutive equation gap method. *Computational Mechanics*, *46*(4), 521-531.

[21] Banerjee, B., Walsh, T. F., Aquino, W., & Bonnet, M. (2013). Large scale parameter estimation problems in frequency-domain elastodynamics using an error in constitutive equation functional. *Computer Methods in Applied Mechanics and Engineering*, *253*, 60-72

[22] Bonnet, M., & Aquino, W. (2014, October). Three-dimensional transient elastodynamic inversion using the modified error in constitutive relation. In

Journal of Physics: Conference Series (Vol. 542, No. 1, p. 012003). IOP Publishing.

[23] Diaz, M. I., Aquino, W., & Bonnet, M. (2015). A modified error in constitutive equation approach for frequency-domain viscoelasticity imaging using interior data. *Computer Methods in Applied Mechanics and Engineering*, *296*, 129-149.

[24] Guchhait, S., & Banerjee, B. (2015). Constitutive error based material parameter estimation procedure for hyperelastic material. *Computer Methods in Applied Mechanics and Engineering*, *297*, 455-475

[25] Wellman, P., Howe, R. D., Dalton, E., & Kern, K. A. (1999). Breast tissue stiffness in compression is correlated to histological diagnosis. *Harvard BioRobotics Laboratory Technical Report*.

[26] Krouskop, T. A., Wheeler, T. M., Kallel, F., Garra, B. S., & Hall, T. (1998). Elastic moduli of breast and prostate tissues under compression. *Ultrasonic Imaging*, *20*(4), 260-274.

[27] Fung Y C (1993). *Biomechanics: Mechanical Properties of Living Tissues* 2nd edn (New York: Springer)

[28] Samani, A., & Plewes, D. (2004). A method to measure the hyperelastic parameters of ex vivo breast tissue samples. *Physics in Medicine and Biology*, *49*(18), 4395.

[29] O'Hagan, J. J., & Samani, A. (2009). Measurement of the hyperelastic properties of 44 pathological ex vivo breast tissue samples. *Physics in Medicine and Biology*, *54*(8), 2557.

[30] Nitta, N., & Shiina, T. (2002). A visualization of nonlinear elasticity property of tissues by ultrasound. *Electronics and Communications in Japan (Part III: Fundamental Electronic Science)*,*85*(12), 9-18.

[31] Erkamp, R. Q., Emelianov, S. Y., Skovoroda, A. R., Chen, X., & O'Donnell, M. (2000, October). Exploiting strain-hardening of tissue to increase contrast in elasticity imaging. In *Ultrasonics Symposium, 2000 IEEE* (Vol. 2, pp. 1833-1836). IEEE.

[32] Erkamp, R. Q., Emelianov, S. Y., Skovoroda, A. R., & O'Donnell, M. (2004). Nonlinear elasticity imaging: theory and phantom study. *Ultrasonics, Ferroelectrics, and Frequency Control, IEEE Transactions on*, *51*(5), 532-539.

[33] Erkamp, R. Q., Emelianov, S. Y., Skovoroda, A. R., & O'Donnell, M. (2002, October). Nonlinear elasticity imaging. In *Ultrasonics Symposium, 2002. Proceedings. 2002 IEEE* (Vol. 2, pp. 1891-1894). IEEE.

[34] Skovoroda, A. R., Lubinski, M., Emelianov, S. Y., & O'Donnell, M. (1999). Reconstructive elasticity imaging for large deformations. *Ultrasonics, Ferroelectrics, and Frequency Control, IEEE Transactions on*, *46*(3), 523-535.

[35] Skovoroda, A. R., Lubinski, M., Emelianov, S. Y., & O'Donnell, M. (1998). Nonlinear estimation of the lateral displacement using tissue incompressibility. *Ultrasonics, Ferroelectrics, and Frequency Control, IEEE Transactions on*, *45*(2), 491-503.

[36] O'Hagan, J. J., & Samani, A. (2009). Measurement of the hyperelastic properties of 44 pathological ex vivo breast tissue samples. *Physics in Medicine and Biology*, *54*(8), 2557.

[37] Samani, A., & Plewes, D. (2004). A method to measure the hyperelastic parameters of ex vivo breast tissue samples. *Physics in Medicine and Biology*, *49*(18), 4395.

[38] Gokhale, N. H., Barbone, P. E., & Oberai, A. A. (2008). Solution of the nonlinear elasticity imaging inverse problem: the compressible case. *Inverse Problems*, *24*(4), 045010.

[39] Goenezen, S., Barbone, P., & Oberai, A. A. (2011). Solution of the nonlinear elasticity imaging inverse problem: The incompressible case. *Computer Methods in Applied Mechanics and Engineering*, *200*(13), 1406-1420.

[40] Goenezen, S., Dord, J. F., Sink, Z., Barbone, P. E., Jiang, J., Hall, T. J., & Oberai, A. A. (2012). Linear and nonlinear elastic modulus imaging: an application to breast cancer diagnosis. *Medical Imaging, IEEE Transactions on*, *31*(8), 1628-1637.

[41] Brezzi, F. (1974). On the existence, uniqueness and approximation of saddle-point problems arising from Lagrangian multipliers. *Revue française d'automatique, informatique, recherche opérationnelle. Analyse numérique*, *8*(2), 129-151.

[42] Maniatty, A. M., Liu, Y., Klaas, O., & Shephard, M. S. (2002). Higher order stabilized finite element method for hyperelastic finite deformation. *Computer Methods in Applied Mechanics and Engineering*, *191*(13), 1491-1503.

[43] Goenezen, S. (2011). Inverse problems in finite elasticity: an application to imaging the nonlinear elastic properties of soft tissues *(Doctoral dissertation)*

[44] Byrd, R. H., Lu, P., Nocedal, J., & Zhu, C. (1995). A limited memory algorithm for bound constrained optimization. *SIAM Journal on Scientific Computing*, *16*(5), 1190-1208.

[45] Vogel, C. R. (2002). *Computational Methods for Inverse Problems* (Vol. 23). Siam.